

Thermalization of open quantum systems using multiple-Davydov D_2 variational approach

Mantas Jakučionis, Darius Abramavičius
*Institute of Chemical Physics, Vilnius University,
Saulėtekio Ave. 9-III, LT-10222 Vilnius, Lithuania*

Numerical implementations of explicit phonon bath require a large number of oscillator modes in order to maintain oscillators at the initial temperature when modelling energy relaxation processes. An additional thermalization algorithm may be useful in controlling the local temperature. In this paper we extend our previously proposed thermalization algorithm [1] to be used with the numerically exact multiple-Davydov D_2 trial wavefunction for simulation of relaxation dynamics and spectroscopic signals of open quantum systems using the time-dependent Dirac-Frenkel variational principle. By applying it to the molecular aggregate model, we demonstrate how the thermalization approach significantly reduces the numerical cost of simulations by decreasing the number of oscillators needed to explicitly simulate the aggregate's environment fluctuations, while maintaining correspondence to the exact population relaxation dynamics. Additionally, we show how the thermalization can be used to find the equilibrium state of the excited molecular aggregate, which is necessary for simulation of the fluorescence and other spectroscopic signals. The presented thermalization algorithm opens possibilities to investigate larger system-bath models than was previously possible using the multiple-Davydov D_2 trial wavefunction and local heating effects in molecular complexes.

I. INTRODUCTION

Open quantum system models are widely used to describe properties of molecular aggregates [2, 3]. The *system* usually consists of molecular electronic states. Intramolecular vibrational degrees of freedom (DOFs), which play the major role in relaxation process of the systems of interest can also be included into the quantum system model. The rest of the DOFs are treated as an environment of a constant temperature – the *bath*. The bath is modelled as a collection of quantum harmonic oscillators (QHO) and is characterized by a continuous fluctuation spectral density function [3–6]. Separation into the system and the bath parts is mostly formal as the system-bath coupling has to be included to account for molecular environment-induced decoherence and temperature effects, hence the quantum dynamics penetrates into the bath, and bath also changes its state.

When using wavefunction-based simulation approaches, it can be challenging to maintain a precise representation of the bath as a constant temperature thermostat, because energy exchange between the system and the bath can alter thermal properties of the bath. Generally, a large number of explicitly modelled QHO modes have to be included to minimize the negative effects of thermal energy accumulation in the bath, but this is numerically expensive. Therefore, one always has to balance between the size of the model, accuracy of the chosen numerical method and its numerical cost. Alternatively, one could numerically change the wavefunction variables during its time evolution in a way as to prevent accumulation of the thermal energy in the bath and to maintain it at a desired temperature, i.e., perform thermalization.

It is challenging to accurately simulate dynamics of quantum systems that exchange energy and (quasi-) par-

ticles with their surroundings, i.e., of the open quantum systems [7, 8], because a numerical cost needed to propagate the corresponding dynamical equations in time increases exponentially with the number of DOFs. The wavefunction approach based on the multiple-Davydov D_2 trial wavefunction (m D_2 ansatz) [9–13], along with the time-dependent variational principle, has been shown to be an excellent tool for accurately simulating the dynamics of system-bath models [9, 14–20] and spectroscopic signals [19–23]. Despite relying on an adaptive, time-dependent state basis set, the problem of rapidly growing numerical costs remain.

In a previous study, we proposed the thermalization algorithm [1] to be used with the Davydov D_2 ansatz [14, 24–29], which restricts QHOs to their lowest uncertainty states – coherent states [30, 31] with Gaussian wavepackets in their coordinate-momentum phase space. We demonstrated how the thermalization algorithm regulates the temperature of the environment and enables the electronically excited molecular system to relax into its equilibrium state at a given temperature [32–34] even when using a reduced number of bath oscillators, which greatly reduces numerical costs. The characteristics of the resulting equilibrium state are essential for modeling fluorescence, excited state emission, excited state absorption and other spectroscopic signals [2]. However, the D_2 ansatz is a crude approximation of the actual system-bath model eigenstates and thus is unable to completely capture electronic population relaxation dynamics [22].

Meanwhile, the system-bath dynamics obtained using the multiple-Davydov ansätze are consistent with the results from other state-of-the-art methods, such as hierarchical equations of motion [10, 12, 22], quasiadiabatic path integral [15], and multi-configuration time-dependent Hartree [16, 35], even when the number of bath oscillators is large. Due to the more complicated

wavefunction structure of the mD₂ ansatz, straightforward application of the D₂ ansatz thermalization algorithm is not possible. In this work, we extend the thermalization algorithm for the mD₂ ansatz by introducing an additional state projection algorithm and adopting the coarse-grained scattering approximation.

In Section (II) we describe the thermalization algorithm for the mD₂ ansatz, and in Section (III) we provide a theoretical description of its application to simulating the fluorescence spectra. Then, in Section (IV) we demonstrate its capabilities by simulating excitation relaxation dynamics of an H-type molecular aggregate and its fluorescence spectrum. Lastly, in Section (V) we discuss changes made to adapt the thermalization algorithm of the D₂ ansatz for the mD₂ ansatz.

II. THERMALIZATION OF THE mD₂ ANSATZ

We consider a molecular aggregate model, where each molecule $n = 1, 2, \dots, N$ couples to its own *local reservoir* $k = 1, 2, \dots, N$, each of which consists of $q = 1, 2, \dots, Q$ QHO modes. The model is given by the Hamiltonian $\hat{H} = \hat{H}_S + \hat{H}_B + \hat{H}_{SB}$ with the system, the bath and the system-bath coupling terms defined as:

$$\hat{H}_S = \sum_n^N \varepsilon_n \hat{a}_n^\dagger \hat{a}_n + \sum_{n \neq m}^{n,m} J_{nm} \hat{a}_n^\dagger \hat{a}_m, \quad (1)$$

$$\hat{H}_B = \sum_{k,q}^{N,Q} \omega_{kq} \hat{b}_{kq}^\dagger \hat{b}_{kq}, \quad (2)$$

$$\hat{H}_{SB} = - \sum_n^N \hat{a}_n^\dagger \hat{a}_n \sum_q^Q \omega_{nq} g_{nq} (\hat{b}_{nq}^\dagger + \hat{b}_{nq}), \quad (3)$$

with the reduced Planck's constant set to $\hbar = 1$. Here ε_n is the n -th molecule electronic excitation energy, J_{nm} denotes the resonant coupling between the n -th and m -th molecules, ω_{nq} denotes the frequency of the q -th QHO in the k -th local reservoir, while g_{nq} is the coupling strength between the q -th oscillator in the n -th local reservoir to the n -th molecule. The operators \hat{a}_n^\dagger and \hat{a}_n represent the creation and annihilation operators for electronic excitations, respectively, while \hat{b}_{nq}^\dagger and \hat{b}_{nq} represent the creation and annihilation bosonic operators for QHOs.

In addition, we implicitly couple the system-bath model to the secondary bath characterized by a fixed temperature, T . The coupling between the secondary and primary baths occurs via the scattering events that allow the system-bath model to exchange energy with the secondary bath and thermalize local reservoirs as is described below.

A state of the system-bath model is given by the mD₂ wavefunction

$$|\Psi(t)\rangle = \sum_{i,n}^{M,N} \alpha_{i,n}(t) |n\rangle \otimes |\lambda_i(t)\rangle, \quad (4)$$

where $\alpha_{i,n}(t)$ is the i -th multiple complex amplitude associated with a singly excited electronic state $|n\rangle$ localized on the n -th molecule, $|n\rangle = \hat{a}_n^\dagger |0\rangle_{el}$. $|0\rangle_{el}$ is the electronic ground state. The complexity and accuracy of the mD₂ ansatz can be adjusted by varying the multiplicity number, M . The states of QHO modes are represented by multi-dimensional coherent states

$$|\lambda_i(t)\rangle = \exp \sum_{k,q}^{N,Q} \left(\lambda_{i,kq}(t) \hat{b}_{kq}^\dagger - \lambda_{i,kq}^*(t) \hat{b}_{kq} \right) |0\rangle_{\text{vib}}, \quad (5)$$

with $\lambda_{i,kq}(t)$ being the i -th multiple complex displacement parameter and $|0\rangle_{\text{vib}} = \otimes_{k,q} |0\rangle_{k,q}$ is the global vibrational ground state of all QHOs.

The mD₂ wavefunction describes a state of the system-bath model as a superposition of M multi-dimensional coherent state terms, which allows it to represent a wide range of system-bath model states beyond the Born-Oppenheimer and Gaussian approximations.

The thermalization algorithm for the mD₂ ansatz is realized by stochastic scattering events [36, 37] during time evolution of the wavefunction. These events change momenta, p_{kq} , of *all* q -th QHO modes of the k -th local reservoir at once. We assume that the scattering probability, $P_k(\theta, \tau_{sc})$, of θ scattering events occurring per time interval, τ_{sc} , with a scattering rate, ν_k , is given by a Poisson distribution

$$P_k(\theta, \tau_{sc}) = \frac{1}{\theta!} (\tau_{sc} \nu_k)^\theta e^{-\tau_{sc} \nu_k}. \quad (6)$$

Numerically, Poisson statistics are realised by simulating Bernoulli processes [38, 39] in the limit of $\tau_{sc} \rightarrow 0$, while maintaining the condition that $\nu_k \tau_{sc} \ll 1$. To simulate the scattering events we divide wavefunction propagation into equal time length, τ_{sc} , intervals

$$t_i = (i\tau_{sc}, (i+1)\tau_{sc}], \quad i = 0, 1, \dots \quad (7)$$

At the end of each interval, for each local reservoir, we flip a biased coin with the probability $\nu_k \tau_{sc}$ of landing *heads* for all local reservoirs. If a k -th coin lands *heads*, we change momenta of *all oscillator modes of that k -th reservoir*, otherwise, no changes are made. A list of scattering moments at which the numerical simulation is paused to perform the scatterings can be precomputed prior to starting the simulation by drawing probabilities for all local reservoir and all time intervals t_i from Eq. (6).

We assume that during the scattering event the local bath, which experiences the scattering, acquires thermal-equilibrium kinetic energy. Such state is given by a single coherent state for one specific QHO. In order to set the new momenta values of the scattered reservoir oscillator modes, we first project the mD₂ wavefunction of Eq. (4) to its single-multiple Davydov D₂ form

$$|\psi(t)\rangle = \sum_n^N \beta_n(t) |n\rangle \otimes |\tilde{\lambda}(t)\rangle, \quad (8)$$

where β_n are the projected complex electronic amplitudes and $|\tilde{\lambda}(t)\rangle$ is the projected multi-dimensional coherent state, which is defined later. This follows the decoherence idea [40], where the macroscopic environment perform a collapse of the wavefunction into a set of preferred states, in our case, the electronic-vibrational states, $|n\rangle \otimes |\tilde{\lambda}(t)\rangle$. The projected complex electronic amplitudes are equal to

$$\beta_n(t) = \sum_i^M \alpha_{i,n}(t) \langle \tilde{\lambda}(t) | \lambda_i(t) \rangle, \quad (9)$$

while the projected multi-dimensional coherent state

$$|\tilde{\lambda}(t)\rangle = \exp \sum_{k,q}^{N,Q} \left(\tilde{\lambda}_{kq}(t) \hat{b}_{kq}^\dagger - \tilde{\lambda}_{kq}^*(t) \hat{b}_{kq} \right) |0\rangle_{\text{vib}} \quad (10)$$

is defined in terms of the complex displacements

$$\tilde{\lambda}_{kq}(t) = \frac{1}{\sqrt{2}} (x_{kq}(t) + ip_{kq}(t)), \quad (11)$$

where $x_{kq}(t)$ and $p_{kq}(t)$ are QHO coordinate and momentum expectation values

$$x_{kq} = \frac{1}{\sqrt{2}} \sum_{i,j,n}^{M,M,N} \alpha_{i,n}^* \alpha_{j,n} \langle \lambda_i | \lambda_j \rangle \sum_{k,q}^{N,Q} (\lambda_{i,kq}^* + \lambda_{j,kq}), \quad (12)$$

$$p_{kq} = \frac{i}{\sqrt{2}} \sum_{i,j,n}^{M,M,N} \alpha_{i,n}^* \alpha_{j,n} \langle \lambda_i | \lambda_j \rangle \sum_{k,q}^{N,Q} (\lambda_{i,kq}^* - \lambda_{j,kq}), \quad (13)$$

calculated from the mD₂ ansatz, where $\langle \lambda_i | \lambda_j \rangle$ is the overlap of two coherent states

$$\langle \lambda_i | \lambda_j \rangle = \exp \sum_{k,q}^{N,Q} \left(\lambda_{i,kq}^* \lambda_{j,kq} - \frac{1}{2} (|\lambda_{i,kq}|^2 + |\lambda_{j,kq}|^2) \right). \quad (14)$$

This completes the projection operation of the mD₂ state, given by Eq. (4), into its simplified D₂ form in Eq. (8).

Once the projected wavefunction is deduced, we modify momenta of the scattered oscillators by sampling the QHO diagonal density operator distribution in the coherent state representation at temperature T , known as the Glauber-Sudarshan distribution [41–44]

$$\mathcal{P}(\tilde{\lambda}_{kq}) = \mathcal{Z}_{kq}^{-1} \exp \left(- \left| \tilde{\lambda}_{kq} \right|^2 \left(e^{\frac{\omega_{kq}}{k_B T}} - 1 \right) \right). \quad (15)$$

For scattered modes, we set momenta values in Eq. (11) to

$$p_{kq}(t) = \sqrt{2} \text{Im} \left(\tilde{\lambda}_{kq}^{\mathcal{P}} \right), \quad (16)$$

where $\tilde{\lambda}_{kq}^{\mathcal{P}}$ is a sample drawn from the Glauber-Sudarshan distribution. \mathcal{Z}_{kq}^{-1} and ω_{kq} are partition functions and frequencies of QHO, respectively, while k_B is the Boltzmann

constant. During the scattering events, coordinates, x_{kq} , of both the scattered and non-scattered modes remain unchanged. Notice, that the local baths, which do not experience scattering, remain unaffected by the scattering of other modes.

Now that the wavefunction of the system-bath model after scattering is known (given by Eq. (8)) we rewrite it in the mD₂ wavefunction form of Eq. (4) by populating amplitudes and displacements of the first multiple, $i = 1$, as

$$\alpha_{1,n}(t) = \beta_n(t), \quad (17)$$

$$\lambda_{1,kq}(t) = \tilde{\lambda}_{kq}(t). \quad (18)$$

Amplitudes of the unpopulated multiples are set to $\alpha_{j=2,\dots,M,n}(t) = 0$, while the unpopulated displacements are positioned in a layered hexagonal pattern around the populated coherent state [19]

$$\lambda_{j=2,\dots,M,kq}(t) = \lambda_{1,kq}(\tau) + \frac{1}{4} (1 + [\beta(j)]) e^{i2\pi(\beta(j) + \frac{1}{12}[\beta(j)])}, \quad (19)$$

where $\beta(j) = (j - 2)/6$ is the coordination function and $[x]$ is the floor function. The exact arrangement of displacements of the unpopulated multiples is not critical, as long as the distance in the phase space to the populated multiple coherent state is not too large, otherwise, the initially unpopulated multiples will not contribute to further dynamics [17, 45].

Once the scattered mD₂ wavefunction is determined and the scattering event is finalised, further simulation of mD₂ dynamics according to equations of motion proceeds. This procedure generates a stochastic wavefunction trajectory, where the system-bath model at each time moment is described by a pure state, which is a single member of a statistical ensemble [42, 43]. The thermalized model dynamics are obtained by averaging observables over an ensemble of wavefunction trajectories, γ , which differ by their: initial amplitudes, $\alpha_{i,n}(0)$, initial coherent state displacements, $\lambda_{i,kq}(0)$, and a sequence of scattering events. Ensemble averaging is performed in a parallelized Monte Carlo scheme.

III. THERMALIZED FLUORESCENCE SPECTRA

Wavefunction trajectories allows calculation of an arbitrary observable. Calculation of equilibrium fluorescence spectrum requires to know thermally equilibrated state of the excited model. The presented thermalization procedure allows to obtain such state and calculate fluorescence spectrum.

In general, the frequency-domain spectrum of a quantum system can be written as a Fourier transform

$$F(\omega) = \text{Re} \int_0^\infty dt e^{i\omega t} S(t), \quad (20)$$

of the corresponding time-domain response function, $S(t)$.

The fluorescence (FL) response function, $S_{\text{fl}}(t)$, is a specific case of the more general time-resolved fluorescence (TRF) response function [2, 46]

$$S_{\text{trf}}(\tau_{\text{eq}}, t) = \frac{1}{\Gamma} \sum_{\gamma=1}^{\Gamma} \langle \Psi_{\text{G}}(0) | \gamma \hat{\mu}_{-} \hat{\mathcal{V}}_{\text{E}}^{\dagger}(\tau_{\text{eq}} + t) \hat{\mu}_{+} \times \hat{\mathcal{V}}_{\text{G}}(t) \hat{\mu}_{-} \hat{\mathcal{V}}_{\text{E}}(\tau_{\text{eq}}) \hat{\mu}_{+} | \Psi_{\text{G}}(0) \rangle_{\gamma}, \quad (21)$$

where $\hat{\mathcal{V}}_{\text{E}}$ and $\hat{\mathcal{V}}_{\text{G}}$ are the excited and ground state system-bath propagators

$$\hat{\mathcal{V}}_A(t_1) | \Psi_A(t_2) \rangle = | \Psi_A(t_1 + t_2) \rangle, \quad (22)$$

while $\hat{\mu}_{+} = \sum_n^N (\mathbf{e} \cdot \boldsymbol{\mu}_n) \hat{a}_n^{\dagger}$ and $\hat{\mu}_{-} = \sum_n^N (\mathbf{e} \cdot \boldsymbol{\mu}_n) \hat{a}_n$ are the excitation creation and annihilation operators of the system [19], $\boldsymbol{\mu}_n$ is the electronic transition dipole moment vector, \mathbf{e} is the external field polarization vector. $|\Psi_{\text{G}}(0)\rangle_{\gamma}$ is a model ground state with an initial condition of the γ -th trajectory. The EOMs for propagating the mD₂ wavefunction, as well as the approach to solving them, are described in detail in Refs. [19, 45].

$S_{\text{trf}}(\tau_{\text{eq}}, t)$ is a function of two times: the equilibration time, τ_{eq} , and the coherence time, t . During the equilibration time, the system evolves in its excited state and, due to the system-bath interaction, relaxes to an equilibrium state. After this, during the coherence time, spontaneous emission occurs.

We will apply thermalization during the equilibration time to facilitate the relaxation of the system-bath model into the lowest energy equilibrium state by removing excess thermal energy from local reservoirs. We denote $\hat{\mathcal{G}}_{\text{E},\gamma}$ as the excited state propagator $\hat{\mathcal{V}}_{\text{E}}$, but with the thermalization. Then the thermalized TRF (tTRF) response function can be written as

$$\tilde{S}_{\text{trf}}(\tau_{\text{eq}}, t) = \frac{1}{\Gamma} \sum_{\gamma=1}^{\Gamma} \langle \Psi_{\text{G}}(0) | \gamma \hat{\mu}_{-} \hat{\mathcal{G}}_{\text{E},\gamma}^{\dagger}(\tau_{\text{eq}}) \hat{\mathcal{V}}_{\text{G}}^{\dagger}(t) \hat{\mu}_{+} \times \hat{\mathcal{V}}_{\text{G}}(t) \hat{\mu}_{-} \hat{\mathcal{G}}_{\text{E},\gamma}(\tau_{\text{eq}}) \hat{\mu}_{+} | \Psi_{\text{G}}(0) \rangle_{\gamma}. \quad (23)$$

By considering the equilibration time to be long enough to reach the equilibrium state of the system-bath model, we define the FL response function to be

$$S_{\text{fl}}(t) = \lim_{\tau_{\text{eq}} \rightarrow \infty} S_{\text{trf}}(\tau_{\text{eq}}, t), \quad (24)$$

and the thermalized fluorescence (tFL) response function as

$$\tilde{S}_{\text{fl}}(t) = \lim_{\tau_{\text{eq}} \rightarrow \infty} \tilde{S}_{\text{trf}}(\tau_{\text{eq}}, t). \quad (25)$$

The spectra obtained using the fluorescence response function without and with thermalization will be compared in the next section. For the numerical simulation, the required equilibration time interval has to be deduced by increasing τ_{eq} until the resulting fluorescence spectra converges.

IV. RESULTS

To investigate the thermalization algorithm for the mD₂ ansatz, we will analyse the linear trimer model, which we previously used to study thermalization of the D₂ ansatz [1]. The model consists of $N = 3$ coupled molecules, with excited state energies ε_n being equal to 0, 250, 500 cm⁻¹, forming an energy funnel. The nearest neighbour couplings are set to $J_{1,2} = J_{2,3} = 100$ cm⁻¹, $J_{3,1} = 0$. The electronic dipole moment vectors of molecules are $\boldsymbol{\mu}_n = (1, 0, 0)$ in Cartesian coordinate system. This classifies the trimer as the H-type molecular aggregate [47].

QHOs of local molecular reservoirs are characterized by the super-Ohmic [48] spectral density function $C''(\omega) = \omega(\omega/\omega_c)^{s-1} \exp(-\omega/\omega_c)$ with an order parameter $s = 2$ and a cut-off frequency $\omega_c = 100$ cm⁻¹. The QHO frequencies are $\omega_{kq} = \omega_0 + (q-1)\Delta\omega$, where the frequency off-set is $\omega_0 = 0.01$ cm⁻¹. The reorganization energy of each local reservoir is $\Lambda_k = \sum_q \omega_{kq} g_{kq}^2 = 100$ cm⁻¹. The scattering time step-size is set to $\tau_{\text{sc}} = 0.01$ ps. Finally, the ensemble consists of 900 wavefunctions trajectories, which we found to be sufficient to obtain the converged model dynamics. The mD₂ ansatz multiplicity $M = 5$ is used as the results with a higher multiplicity quantitatively match the $M = 5$ case.

We will be considering three bath models: the *dense bath* model, where the spectral density function $C''(\omega)$ is discretized into $Q = 75$ oscillators per local reservoir with a step-size of $\Delta\omega = 10$ cm⁻¹; the *sparse bath* model, where the number of modes is reduced by a factor of 5 to just $Q = 15$ oscillators per local reservoir with $\Delta\omega = 50$ cm⁻¹; and the *sparse bath with thermalization* model, where $C''(\omega)$ is discretized according to the sparse bath model and thermalization is used.

In the absence of the bath, the system has three single-excitation stationary exciton states with energies: $E_1^{\text{exc}} \approx -37.23$ cm⁻¹, $E_2^{\text{exc}} = 250$ cm⁻¹, $E_3^{\text{exc}} \approx 537.23$ cm⁻¹, satisfying the time-independent Schrödinger equation

$$\hat{H}_{\text{S}} \Phi_n^{\text{exc}} = E_n^{\text{exc}} \Phi_n^{\text{exc}}, \quad (26)$$

with the system Hamiltonian given by Eq. (1). The exciton eigenstates [3, 5], Φ_n^{exc} , have their excitations delocalized over multiple molecules [42]. Therefore, it is convenient to analyse molecular aggregate excitation relaxation dynamics in terms of excitons as they are natural quasi-particles of the aggregate. We denote the probability of finding the aggregate in its n -th excitonic state as the population, given by

$$\rho_n^{\text{exc}}(t) = \sum_{k,l,i,j} (\Phi_k^{\text{exc}})_n^* \langle \alpha_{i,k}^*(t) \alpha_{j,l}(t) S_{i,j}(t) \rangle_{\text{th}} (\Phi_l^{\text{exc}})_n, \quad (27)$$

where $\langle \dots \rangle_{\text{th}}$ is the averaging over an ensemble of wavefunction trajectories.

Using mD₂ ansatz we have

First, we study the electronic excitation dynamics. The initial excitonic state populations correspond to the

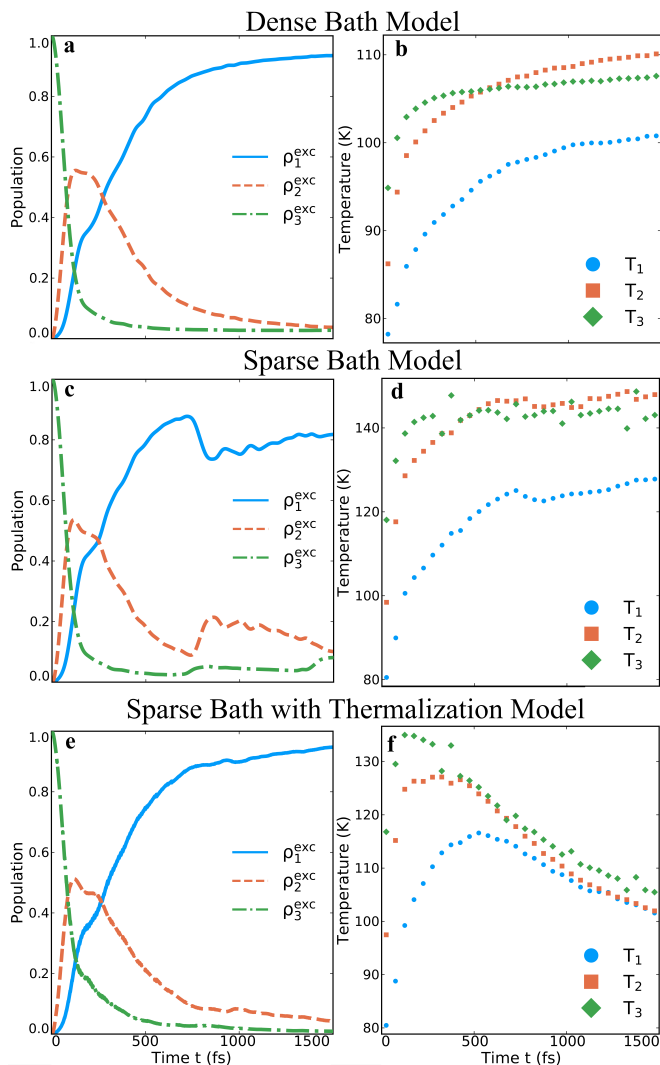


Figure 1. The exciton state populations, $\rho_n^{\text{exc}}(t)$, and the average temperatures, $T_k(t)$, of local reservoirs of the trimer with (a, b) the dense bath model, (c, d) the sparse bath model and (e, f) the sparse bath model with thermalization.

optically excited highest energy state: $\rho_3^{\text{exc}} = 1$, $\rho_{1,2}^{\text{exc}} = 0$, while the initial QHO displacements, $\lambda_{i,kq}(0)$, are sampled from the Glauber-Sudarshan distribution in Eq. (15) to account for the initial temperatures of $T_k = 77$ K.

In Fig. (1) we display the trimer model exciton state populations $\rho_n^{\text{exc}}(t)$ and average temperatures [49] $T_k(t)$ of local reservoirs for all three bath models. The aggregate environment causes dephasing between excitonic states and induces irreversible population relaxation [2, 3]. The population dynamics of the dense bath models exhibits a sequential relaxation from the initially populated highest energy excitonic state to the lowest energy state via the intermediate state. Eventually, the population distribution reaches the equilibrium state. The majority of the excitation energy is transferred to oscillators of local reservoirs. We observe an increase of temperatures [49–51] due to the finite num-

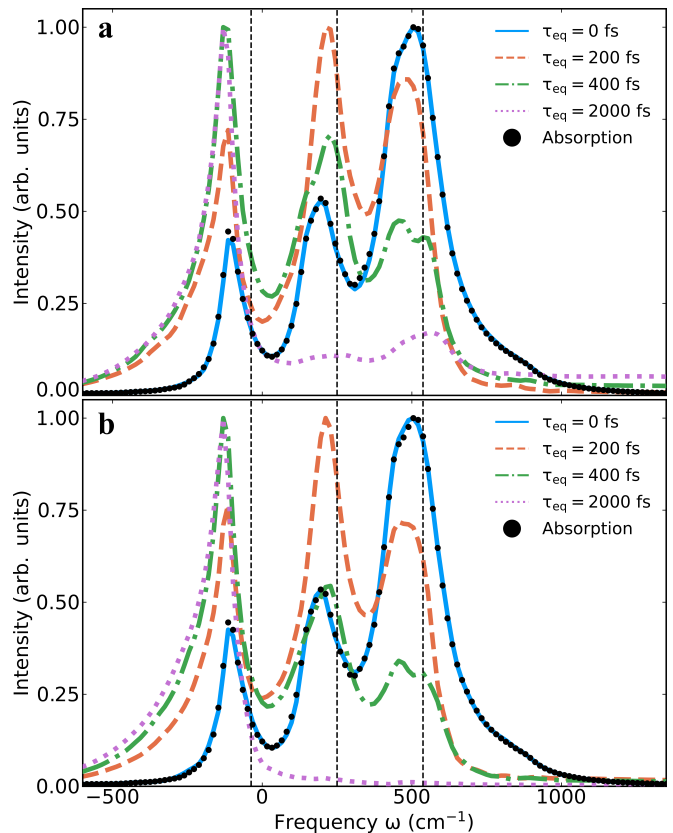


Figure 2. (a) the TRF and (b) tTRF spectra of the trimer with the dense bath model, simulated with an increasing equilibration time τ_{eq} . The absorption spectrum is also shown. Vertical dashed lines show energies E^{exc} of the excitonic states.

ber of oscillators in local reservoirs. An infinite number of oscillators would have to be included to maintain temperature constant at the initial value. The initial rapid rise in temperature is due to oscillator reorganization in the aggregate’s electronic excited state manifold, while the following slow rise is due to energy transfer from the system to local reservoirs.

In the sparse bath model, we observe that if the number of vibrational modes is reduced, the population dynamics become skewed due to insufficiently dense representation of the spectral density function. Furthermore, the temperature increase is higher than compared to the dense bath model, which further changes the characteristics of the resulting equilibrium state.

When the thermalization algorithm is applied to the sparse bath model with a scattering rate $\nu_k = 1.25$ ps $^{-1}$, the population dynamics are restored and qualitatively match those of the dense model. Although the initial temperatures of the local reservoirs exceed those of the dense bath model, they gradually decrease due to thermalization, and this rate can be adjusted by changing the scattering rate.

Next, we turn our attention to simulating the FL spectrum of the linear trimer with the dense bath model with

scattering rate $\nu_k = 1 \text{ ps}^{-1}$. The initial excitonic state population distribution is now calculated in terms of the system-field interaction, as described in Ref. [19].

In Fig. (2) we compare the TRF and tTRF spectra with increasing equilibration times τ_{eq} . When $\tau_{\text{eq}} = 0$, both the TRF and tTRF spectra are equivalent and exactly match the absorption spectrum, which consists of three peaks due to transition involving the combined excitonic-vibronic (vibronic) states and can not be regarded as purely excitonic. For reference, vertical dotted lines indicate energies E^{exc} of excitonic states. These do not match the three peak energies exactly due to the system being coupled to the environment.

By allowing equilibration to occur, $\tau_{\text{eq}} > 0$, both the TRF and tTRF spectra show peak intensity shift towards lower energies as excitation relaxes towards the equilibrated state during the equilibration time. After equilibrating for $\tau_{\text{eq}} = 2 \text{ ps}$, we find that both spectra have converged and do not change with longer τ_{eq} . Therefore, the TRF and tTRF spectra at $\tau_{\text{eq}} = 2 \text{ ps}$ can be considered as the FL and tFL spectra of the trimer model as defined in Eqs. (24), (25).

Both spectra exhibit their highest intensities at the energies of the lowest vibronic states. However, the FL spectrum also has considerable intensities at energies of the intermediate and highest vibronic states. Surprisingly, the higher energy peak is more intense than the intermediate peak. The tFL spectrum intensities at these energies are negligible, which indicate that the thermalization allows the trimer model to reach a lower energy equilibrium state, which is no longer hindered by the excess thermal energy accumulation in QHOs of local reservoirs.

In Fig. (3), we also compare the obtained FL and tFL spectra with the FL spectrum simulated using a previously proposed excited state numerical optimization approach [20, 52, 53]. It relies on finding the model's lowest energy excitonic state in terms of the mD₂ ansatz parameters and then applying thermal fluctuations to effectively generate the model in a lowest energy equilibrium state at the temperature of 77 K. We see that all three methods produce a similar lowest vibronic peak, but the tFL spectrum has a higher intensity tail towards the low energy side and almost no intensities at energies of the intermediate and the highest vibronic states, while the FL spectrum simulated using the optimization approach has a small intensity at the energy of the intermediate vibronic states. The optimization approach spectrum more closely resembles that of the thermalized model than the non-thermalized spectrum.

V. DISCUSSION

Starting from an arbitrary non-equilibrium initial condition a closed quantum system will not equilibrate due to energy conservation. Thermalization procedure is necessary to guarantee proper thermal equilibrium in the

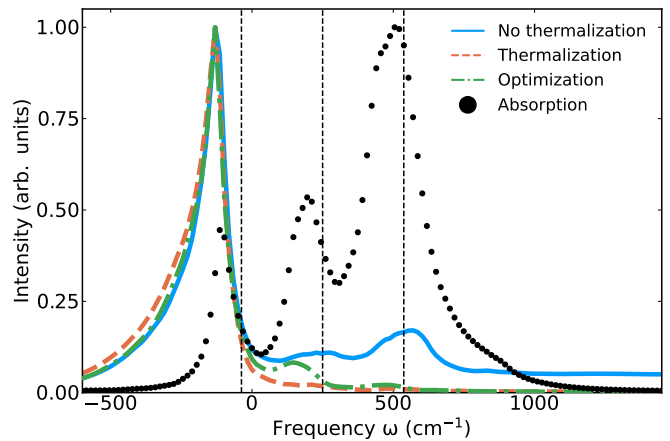


Figure 3. The fluorescence spectra comparison of the trimer with the dense bath model obtained without thermalization, with thermalization and using the optimization approach. The equilibration time is $\tau_{\text{eq}} = 2 \text{ ps}$. The absorption spectrum is also shown. Vertical dashed lines show energies E^{exc} of the excitonic states.

long run for *all* bath oscillators. This requires introducing the concept of primary and secondary baths. In our model the primary bath is a part of explicit quantum DOFs, while the secondary bath is a thermal reservoir with infinite thermal capacity, i. e. it keeps constant temperature in any energy exchange process. In this case, the secondary bath cannot be described by mechanical equations – only statistical or thermodynamical concepts apply. Our statistical algorithm performs energy exchange between the primary and secondary baths using the statistical scattering idea: the primary bath state is being reset to the thermally equilibrated state, thus giving up excess energy to or drawing additional energy from the secondary bath. This is a major extension of the explicit quantum TDVP theory – the extended model covers a broader range of phenomena: local heating and cooling, as well as bath oscillator dynamic localization, which are not available in the standard TDVP theory.

In order to adapt the D₂ ansatz thermalization algorithm for the mD₂ ansatz, several extensions were made. During the time evolution of the system-bath model, the mD₂ ansatz multiples become correlated, leading to a non-Gaussian bath wavefunction. It becomes impossible to represent a new Gaussian wavefunction of scattered QHO modes, sampled from Eq. (15), without changing the wavefunction of all the rest non-scattered oscillators at the same time. Therefore, we chose to project the mD₂ into the D₂ ansatz whenever scatterings occurs, allowing to correctly represent the newly sampled Gaussian wavefunction of scattered oscillators. This idea requires the consideration of a few aspects.

The projected D₂ wavefunction accurately maintains *average* coordinates and momenta of the mD₂ ansatz QHO states, while variances and higher-order moments become affected. This causes variation of excitation relaxation dynamics compared to the standard mD₂

ansatz. However, system-bath models mostly rely only on the *linear* coupling between the system and average coordinates of QHO modes, therefore, as seen in Fig. (1), the discrepancy is minimal. The higher-order couplings become necessary when anharmonic vibrational modes or changes to their frequencies upon excitation are considered [20, 54].

To maintain the close correspondence to the standard mD₂ ansatz the projection should not occur too often. This is because it takes time for the wavefunction after scattering to again become correlated between its many multiples, i.e., to take advantage of the unpopulated mD₂ ansatz multiples after projection. If the repopulation time is shorter than the time between projection operations, the model population dynamics become similar to those of the D₂ ansatz, even though the mD₂ ansatz is being used. The average time interval between projection operations is determined by the scattering rate ν_k , a property of the physical system, while the scattering time τ_{sc} is a parameter of the model and must be as small as necessary to ensure the Bernoulli-to-Poisson statistics transition condition, $\nu_k \tau_{sc} \ll 1$.

To increase the average time between projection operations, we adopt a coarser scattering approach for the mD₂ ansatz as compared to the D₂ ansatz. Instead of considering scattering events of individual oscillators, we consider events, where all oscillators of certain local reservoirs are scattered at once, requiring only a single projection operation to scatter many oscillators at once. This approach allows the mD₂ ansatz to continue utilizing all its multiples for the improved accuracy over the D₂ ansatz, while reducing the number of explicitly modelled oscillators needed to maintain local reservoirs' temperatures close to initial values, thereby reducing the numerical cost.

Using the mD₂ ansatz to simulate population dynamics of the trimer model, it took an average of 166 minutes per trajectory using the dense bath model, but only 1.3 minutes using the sparse bath model and 2 minutes using the sparse bath model with thermalization. The computational overhead of thermalization is small compared to the overall time savings when switching from using the dense bath to the sparse bath. The numerical cost reduction is also greater for the mD₂ ansatz than for the D₂ ansatz in Ref. [1], because the mD₂ ansatz EOMs constitute an *implicit* system of differential equations, which require a more involved, two-step numerical approach to find a solution [19, 45]. By considering fewer oscillators in each local reservoir, simulations of the dynamics and spectroscopic signals of aggregates made up of more molecules becomes possible.

Computing a single trajectory of the tTRF response

function in Eq. (23) with an equilibration time of $\tau_{eq} = 2$ ps took an average of 79 minutes. The previously proposed optimization method [20] for simulating FL spectra does not require propagation during the equilibration time interval of the TRF response function and has to be computed only once, but it took 193 minutes. In general, we find that the computation of tTRF is more reliable and numerically stable. The optimization approach struggles to consistently find the lowest energy excitonic state of the model due to its heuristic nature, requiring many attempts to find the solution and eventually having to choose the lowest energy one. This is particularly apparent when a wide range of oscillator frequencies are included.

For elementary system-bath models without Hamiltonian parameter disorder, the optimization approach can be a good starting point for FL spectra simulation. However, a more accurate spectra most likely will be obtained using the tTRF approach. For models with Hamiltonian disorder, e.g., static molecule excitation energy disorder [55–57], the optimization approach would require finding model's lowest energy excitonic state for each realization of the Hamiltonian, negating its advantage of having to perform optimization procedure only once.

In conclusion, the presented thermalization algorithm for the numerically exact mD₂ ansatz allows to reduce numerical cost of system-bath model simulations by having to explicitly include fewer bath oscillators, while maintaining correspondence with the exact relaxation dynamics. The thermalization algorithm efficiently controls molecular heating effects due to the reduced number of oscillators. Furthermore, the application of thermalization to simulation of fluorescence spectra demonstrates lower computation time, greater numerical stability and higher accuracy compared to the numerical optimization approach.

CONFLICTS OF INTEREST

There are no conflicts of interest to declare.

ACKNOWLEDGMENTS

We thank the Research Council of Lithuania for financial support (grant No: S-MIP-23-48). Computations were performed on resources at the High Performance Computing Center, “HPC Sauletekis” in Vilnius University Faculty of Physics.

[1] M. Jakučionis and D. Abramavičius, Temperature-controlled open-quantum-system dynamics using a time-dependent variational method, *Physical Review A* **103**, 032202 (2021).

[2] S. Mukamel, *Principles of nonlinear optical spectroscopy* (Oxford University Press, 1995).

[3] L. Valkunas, D. Abramavičius, and T. Mančal, *Molecular Excitation Dynamics and Relaxation* (Wiley-VCH Verlag

- GmbH, 2013).
- [4] C. J. Bardeen, The Structure and Dynamics of Molecular Excitons, *Annual Review of Physical Chemistry* **65**, 127 (2014).
 - [5] H. van Amerongen, R. van Grondelle, and L. Valkunas, *Photosynthetic Excitons* (World Scientific, 2000).
 - [6] M. Schröter, S. Ivanov, J. Schulze, S. Polyutov, Y. Yan, T. Pullerits, and O. Kühn, Exciton-vibrational coupling in the dynamics and spectroscopy of Frenkel excitons in molecular aggregates, *Physics Reports* **567**, 1 (2015).
 - [7] H.-P. Breuer and F. Petruccione, *The Theory of Open Quantum Systems* (Oxford University Press, 2007).
 - [8] U. Weiss, *Quantum Dissipative Systems* (WORLD SCIENTIFIC, 2012).
 - [9] N. Zhou, Z. Huang, J. Zhu, V. Chernyak, and Y. Zhao, Polaron dynamics with a multitude of Davydov D 2 trial states, *The Journal of Chemical Physics* **143**, 014113 (2015).
 - [10] L. Wang, L. Chen, N. Zhou, and Y. Zhao, Variational dynamics of the sub-Ohmic spin-boson model on the basis of multiple Davydov D 1 states, *The Journal of Chemical Physics* **144**, 024101 (2016).
 - [11] N. Zhou, L. Chen, Z. Huang, K. Sun, Y. Tanimura, and Y. Zhao, Fast, Accurate Simulation of Polaron Dynamics and Multidimensional Spectroscopy by Multiple Davydov Trial States, *Journal of Physical Chemistry A* **120**, 1562 (2016).
 - [12] L. Chen, M. Gelin, and Y. Zhao, Dynamics of the spin-boson model: A comparison of the multiple Davydov D1,D1.5,D2 Ansätze, *Chemical Physics* **515**, 108 (2018).
 - [13] Y. Zhao, K. Sun, L. Chen, and M. Gelin, The hierarchy of Davydov's Ansätze and its applications, *WIREs Computational Molecular Science* **12**, e1589 (2022).
 - [14] Z. Huang, L. Chen, N. Zhou, and Y. Zhao, Transient dynamics of a one-dimensional Holstein polaron under the influence of an external electric field, *Annalen der Physik* **529**, 1600367 (2017).
 - [15] L. Wang, Y. Fujihashi, L. Chen, and Y. Zhao, Finite-temperature time-dependent variation with multiple Davydov states, *J. Chem. Phys.* **146**, 124127 (2017).
 - [16] L. Chen, M. F. Gelin, and W. Domcke, Multimode quantum dynamics with multiple Davydov D2 trial states: Application to a 24-dimensional conical intersection model, *Journal of Chemical Physics* **150**, 24101 (2019).
 - [17] M. Jakučionis, T. Mancal, and D. Abramavičius, Modeling irreversible molecular internal conversion using the time-dependent variational approach with sD2 ansatz, *Physical Chemistry Chemical Physics* **22**, 8952 (2020).
 - [18] L. Wang, F. Zheng, J. Wang, F. Großmann, and Y. Zhao, Schrödinger-Cat States in Landau-Zener-Stückelberg-Majorana Interferometry: A Multiple Davydov Ansatz Approach, *Journal of Physical Chemistry B* **125**, 3184 (2021).
 - [19] M. Jakučionis, A. Žukauskas, and D. Abramavičius, Modeling molecular J and H aggregates using multiple-Davydov D2 ansatz, *Physical Chemistry Chemical Physics* **24**, 17665 (2022).
 - [20] M. Jakučionis, A. Žukauskas, and D. Abramavičius, Inspecting molecular aggregate quadratic vibronic coupling effects using squeezed coherent states, *Physical Chemistry Chemical Physics* **25**, 1705 (2023).
 - [21] K. W. Sun, M. F. Gelin, V. Y. Chernyak, and Y. Zhao, Davydov Ansatz as an efficient tool for the simulation of nonlinear optical response of molecular aggregates, *Journal of Chemical Physics* **142**, 212448 (2015).
 - [22] N. Zhou, L. Chen, Z. Huang, K. Sun, Y. Tanimura, and Y. Zhao, Fast, Accurate Simulation of Polaron Dynamics and Multidimensional Spectroscopy by Multiple Davydov Trial States, *Journal of Physical Chemistry A* **120**, 1562 (2016).
 - [23] Y. Zhao, The hierarchy of Davydov's Ansätze: From guesswork to numerically "exact" many-body wave functions, *Journal of Chemical Physics* **158**, 80901 (2023).
 - [24] J. Sun, B. Luo, and Y. Zhao, Dynamics of a one-dimensional Holstein polaron with the Davydov ansätze, *Physical Review B - Condensed Matter and Materials Physics* **82**, 014305 (2010).
 - [25] B. Luo, J. Ye, C. Guan, and Y. Zhao, Validity of time-dependent trial states for the Holstein polaron, *Physical Chemistry Chemical Physics* **12**, 15073 (2010).
 - [26] M. Jakučionis, V. Chorošajev, and D. Abramavičius, Vibrational damping effects on electronic energy relaxation in molecular aggregates, *Chemical Physics* **515**, 193 (2018).
 - [27] M. Jakucionis, I. Gaiziunas, J. Sulskus, and D. Abramavičius, Simulation of Ab Initio Optical Absorption Spectrum of β -Carotene with Fully Resolved S0 and S2 Vibrational Normal Modes, *The Journal of Physical Chemistry A* **126**, 180 (2022).
 - [28] A. S. Davydov, Solitons in molecular systems, *Physica Scripta* **20**, 387 (1979).
 - [29] A. C. Scott, Davydov's soliton revisited, *Physica D: Non-linear Phenomena* **51**, 333 (1991).
 - [30] W.-M. Zhang, D. H. Feng, and R. Gilmore, Coherent states: Theory and some applications, *Rev. Mod. Phys* **62**, 867 (1990).
 - [31] S. Kais and R. D. Levine, Coherent states for the Morse oscillator, *Phys. Rev. A* **41**, 2301 (1990).
 - [32] J. M. Moix, Y. Zhao, and J. Cao, Equilibrium-reduced density matrix formulation: Influence of noise, disorder, and temperature on localization in excitonic systems, *Phys. Rev. B* **85**, 115412 (2012).
 - [33] Y. Subasi, C. H. Fleming, J. M. Taylor, and B. L. Hu, Equilibrium states of open quantum systems in the strong coupling regime, *Phys. Rev. E* **86**, 061132 (2012).
 - [34] A. Gelzinis and L. Valkunas, Analytical derivation of equilibrium state for open quantum system, *The Journal of Chemical Physics* **152**, 051103 (2020).
 - [35] J. Zeng and Y. Yao, Variational Squeezed Davydov Ansatz for Realistic Chemical Systems with Nonlinear Vibronic Coupling, *Journal of Chemical Theory and Computation* **18**, 1255 (2022).
 - [36] M. B. Plenio and P. L. Knight, The quantum-jump approach to dissipative dynamics in quantum optics, *Reviews of Modern Physics* **70**, 101 (1998).
 - [37] K. Luoma, W. T. Strunz, and J. Piilo, Diffusive Limit of Non-Markovian Quantum Jumps, *Physical Review Letters* **125**, 150403 (2020).
 - [38] V. N. Kampen, *Stochastic Processes in Physics and Chemistry* (Elsevier, 2007).
 - [39] D. Bertsekas and J. Tsitsiklis, Introduction to probability, in *Introductory Medical Statistics* (IOP Publishing Ltd, 2008).
 - [40] M. Schlosshauer, *Decoherence and the Quantum-To-Classical Transition* (Springer Berlin Heidelberg, Berlin, Heidelberg, 2007).

- [41] R. J. Glauber, Coherent and incoherent states of the radiation field, *Physical Review* **131**, 2766 (1963).
- [42] V. Chorošajev, O. Rancova, and D. Abramavicius, Polaronic effects at finite temperatures in the B850 ring of the LH2 complex, *Physical Chemistry Chemical Physics* **18**, 7966 (2016).
- [43] L. Wang, Y. Fujihashi, L. Chen, and Y. Zhao, Finite-temperature time-dependent variation with multiple Davydov states, *The Journal of Chemical Physics* **146**, 124127 (2017).
- [44] Q. Xie, H. Zhong, M. T. Batchelor, and al, Including temperature in a wavefunction description of the dynamics of the quantum Rabi model, *Journal of Physics A: Mathematical and Theoretical* **51**, 014001 (2017).
- [45] M. Werther and F. Großmann, Apoptosis of moving nonorthogonal basis functions in many-particle quantum dynamics, *Physical Review B* **101**, 174315 (2020).
- [46] V. Balevičius, L. Valkunas, and D. Abramavicius, Modeling of ultrafast time-resolved fluorescence applied to a weakly coupled chromophore pair, *The Journal of Chemical Physics* **143**, 074101 (2015).
- [47] N. J. Hestand and F. C. Spano, Expanded Theory of H- and J-Molecular Aggregates: The Effects of Vibronic Coupling and Intermolecular Charge Transfer, *Chemical Reviews* **118**, 7069 (2018).
- [48] A. Kell, X. Feng, M. Reppert, and R. Jankowiak, On the shape of the phonon spectral density in photosynthetic complexes, *Journal of Physical Chemistry B* **117**, 7317 (2013).
- [49] D. Abramavicius, V. Chorošajev, and L. Valkunas, Tracing feed-back driven exciton dynamics in molecular aggregates, *Physical Chemistry Chemical Physics* **20**, 21225 (2018).
- [50] V. Scarani, M. Ziman, P. Štelmachovič, N. Gisin, and V. Bužek, Thermalizing Quantum Machines: Dissipation and Entanglement, *Physical Review Letters* **88**, 097905 (2002).
- [51] A. W. Chin, J. Prior, R. Rosenbach, F. Caycedo-Soler, S. F. Huelga, and M. B. Plenio, The role of non-equilibrium vibrational structures in electronic coherence and recoherence in pigment-protein complexes, *Nature Physics* **9**, 113 (2013).
- [52] P. K Mogensen and A. N Riseth, Optim: A mathematical optimization package for Julia, *Journal of Open Source Software* **3**, 615 (2018).
- [53] Z. H. Zhan, J. Zhang, Y. Li, and H. S. Chung, Adaptive particle swarm optimization, *IEEE transactions on systems, man, and cybernetics. Part B, Cybernetics : a publication of the IEEE Systems, Man, and Cybernetics Society* **39**, 1362 (2009).
- [54] V. Chorošajev, T. Marčiulionis, and D. Abramavicius, Temporal dynamics of excitonic states with nonlinear electron-vibrational coupling, *The Journal of Chemical Physics* **147**, 074114 (2017).
- [55] D. Abramavicius and L. Valkunas, Geminate pair recombination in molecular systems with correlated disorder, *Physical Review B* **68**, 245203 (2003).
- [56] A. Eisfeld, S. M. Vlaming, V. A. Malyshev, and J. Knoester, Excitons in molecular aggregates with lévy-type disorder: Anomalous localization and exchange broadening of optical spectra, *Physical Review Letters* **105**, 137402 (2010).
- [57] O. Rancova, M. Jakučionis, L. Valkunas, and D. Abramavicius, Origin of non-Gaussian site energy disorder in molecular aggregates, *Chemical Physics Letters* **674**, 120 (2017).